# Silicon Nano-Particles Doped Optical Fiber: Fabrication, Characterization, and Application

A. V. Kir'yanov, *Member, IEEE, Senior Member, OSA*, M. C. Paul, *Member, IEEE*, Yu O. Barmenkov, *Member, IEEE*, A. M. Martínez-Gamez, S. Das, M. Pal, J. L. Lucio-Martínez, A. Arredondo-Santos, V. A. Kamynin, and V. G. Plotnichenko

***Abstract*—The fabrication of a new-type of Silicon nanoparticles (Si-n/p) doped silica fiber is reported. The method is entirely based on the MCVD process, with no solution-doping technique being required. The TEM, EPMA, EDX, and electron diffraction analyses as well as the Raman, optical absorption, and fluorescence spectra' measurements confirm the formation of Si-n/p in the fiber. When pumped at 406 nm, this fiber fluoresces mainly in the VIS to near-IR spectral range and the fluorescence shows a multi-peak spectral structure in several wide bands. As a consequence of the high nonlinearity $n_2$ of the fiber, effective supercontinuum generation at 1.6-$\mu$m excitation by tens ns-range, kW-level pulses is demonstrated.**

***Index Terms*—Fiber optics, MCVD, nanoparticles, nonlinear refractive index, silicon, supercontinuum.**

## I. Introduction

NANO-SIZED Silicon (Si) is known to produce interesting and invaluable effects for practical applications, in particular the quantum confinement phenomenon. So far many reports focused on the functioning features of nano-sized Si in the form of nanoparticles (Si-n/p) embedded within silica matrix. It was particularly shown that Si in the form of Si-n/p produces outstanding enhancement of fluorescence, mainly in VIS to near-IR spectral region (see e.g. reviews [1]–[4]), and a strong increase in the nonlinear-optical properties (see e.g. remarkable papers [5]–[8]).

Manuscript received July 12, 2012; revised February 21, 2013; accepted March 24, 2013. Date of publication April 12, 2013; date of current version May 03, 2013. This work was supported in part by the Programme of Cooperation in Science and Technology between India and Mexico. The work of M. C. Paul, S. Das, and M. Pal was supported in part by the Council of Scientific and Industrial Res23earch (CSIR)-INDIA through the EMPOWER Project.

A. V. Kir'yanov is with the Centro de Investigaciones en Optica Leon 37150, Guanajuato, Mexico. He is also with the Physics Department of M.V. Lomonosov Moscow State University, Vorobyevy Gory, Moscow 119991, Russian Federation (e-mail: kiryanov@cio.mx; alejandrokir@gmail.com).

M. C. Paul, S. Das, and M. Pal are with the Fiber Optics and Photonic Division, Central Glass & Ceramic Research Institute-CSIR Kolkata-700 032, India (e-mail: mcpal@cgcri.res.in).

Y. O. Barmenkov, and A. M. Martínez-Gamez are with the Centro de Investigaciones en Optica, Leon 37150, Guanajuato, Mexico.

J. L. Lucio-Martínez and A. Arredondo-Santos are with the Division de Ciencias e Ingenierías de la Universidad de Guanajuato, Leon 37150, Guanajuato, Mexico.

V. A. Kamynin is with A.M. Prokhorov General Physics Institute of the Russian Academy of Science, Moscow 119991, Russia.

V. G. Plotnichenko is with the Fiber Optics Research Center of the Russian Academy of Sciences, Moscow 119991, Russia. He is also with the Moscow Institute of Physics and Technology Moscow Region, 141700, Russia.

Color versions of one or more of the figures in this paper are available online at http://ieeexplore.ieee.org.

Digital Object Identifier 10.1109/JLT.2013.2257682

Recently, attention has been also attracted by silica fibers doped with Si-n/p since the main properties of Si-n/p—measured at the preform stage—may be preserved through fabricating procedure and also observed in a drawn fiber. When Si-n/p are embedded within fiber's core (at the scale of tens of $\mu$m) then the long interaction distance at light propagation [9], [10] and the strong confinement of an optical field results in enhancement of the fluorescent and nonlinear-optical properties of the system.

As far as we know, only few results have been published regarding the fabrication and characterization of Si-n/p fibers; see [11]–[16].

S. Moon *et al.* [11], [12] and P.R. Watekar *et al.* [13] reported on fabrication of Si-n/p fiber through the modified chemical vapor deposition (MCVD) process, followed by the solution doping (SD) technique, where the doping solutions used were prepared by mixing 0.3 g of the crushed Si-powders (Kojundo: SIE17PB) and/or $ErCl_3\ 6H_2O$ and $AlCl_3\ 6H_2O$ with ethanol for 12 hours. In this case, the porous layers for the core were first deposited on the inner surface of a high-purity silica glass tube by means of the MCVD process using vaporized $SiCl_4$ and $GeCl_4$ as precursor chemicals. Then the core layers were partially sintered at 1650°C by the oxy/hydrogen burner to prevent the layers breakdown during the SD process. After the partial sintering of the core layers, the porous region was soaked with the doping solution for 1 hour at room temperature. In this technique, no Si-n/p developed within the system *in-situ*. The externally used Si-powder in solution was incorporated into silica glass matrix through soaking process of porous layer, which is ineffective for the uniform incorporation of Si-n/p along the fiber length and within its core area unless porosity becomes uniform along the whole deposition length. Furthermore, the SD process gives rise to disturbance of porous layer during dipping into solution, if not maintained the proper uniform temperature. G. Brasse *et al.* [14], [15] reported on fabrication of other nanostructured $SiO_2 - ZrO_2$-based fiber with and without rare-earths through the chemical sol-gel technique where the fabrication parameters and the material characterization results were provided. It was shown that the sol-gel technique may be a route for making of Si-n/p doped fiber, too. However, such a process seems to be very long-time consuming matter. K. Mantey *et al.* [16] reported on using another process, known as wet treatment, for immobilizing luminescent Si-n/p in industrial fibers to impart their optical and chemical functions but also without creating of Si-n/p *in-situ*.

On contrary, we have developed the technological process for incorporation of Si-n/p *in-situ*, without applying the SD

technique. This is the main novelty of our approach. As well, we present for the Si-n/p fiber the results of transmission electron microscopy (TEM) analysis together with the data of energy-dispersive X-ray (EDX) spectroscopy and electron-diffraction measurements to support the presence of nanoparticles within the fiber core, which is absent in the above referred results [11]–[16]. Our main motivation was attempting an original, simple but effective route to develop Si-n/p doped fibers. The present paper reports the current state-of-the-art in the development, characterization in terms of basic optical properties, and application (supercontinuum generation) of such fiber. Despite being currently a for-lab instrument, our facilities are capable for producing at least 2 km of the fiber, drawn from a ∼50-cm preform length. The reported results reveal that such Si-n/p fibers promise to impact telecommunication systems and would become an active medium for amplifying applications.

## II. Fabrication of Si-n/p Preform and Fiber

Fabrication of optical fibers doped with Si-n/p sized by few to tens nm, using the standard MCVD method, exhibits much interest for future innovative applications. As our preliminary insight to the matter revealed, this needs certain skills as for obtaining on-demand optical preforms, as for making final fibers doped with Si-n/p.

The technologies so far employed for the incorporation of Si-n/p into optical fibers are essentially different from the one to be reported below. The main innovation based on the knowledge of material chemistry has allowed us to make Si-n/p doped preforms by employing solely a MCVD process, not by means of the SD technique always applied earlier.

It was predominantly clear that suitable dopant precursors should be chosen for making a fiber preform, which favors the formation of Si-n/p within the silica matrix using the conventional MCVD technology, followed by an optimized thermal treatment of the preform. Optimization of a suitable host glass composition and the preform fabrication parameters was then made for keeping the size of Si-n/p within a 1–10 nm range.

In the route of a preform's fabrication, vapor of $SiCl_4$ is introduced into a rotating silica tube with radial dimensions 20/17 mm, under certain flow of high purity helium gas through a mass flow controller at 15.0 psig pressure. Aluminium (Al) vapor is generated by heating the inlet silica tube (at around 1200–1400°C), inside of which Al foil or wires of high purity (99.999%) is wrapped, using a hand torch burner. Al vapor reduces $SiCl_4$ in the presence of high purity helium gas, which proceeds through the following chemical reaction:

$$3SiCl_4(vapor)+4Al(vapor) = 3Si(Solid+4AlCl_3(vapor).$$

Such deposition process that occurs at temperatures 1400–1450°C is illustrated by Fig. 1.

It should be noted that some portion of $SiCl_4$ could form $SiO_2$ during the deposition if inside environment of the reaction tube is not entirely inert. Thus, prevention from oxidation of Si to $SiO_2$ was achieved through maintaining possibly high inertial atmosphere within the deposition tube. Also of mention is that flow of $O_2$ (10–15%) ought to be used to prevent formation of carbon, which would come from the thermal decomposition reaction of hydrocarbon compounds.

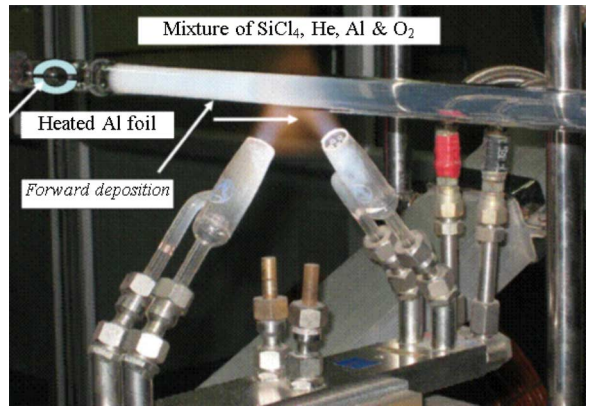


Fig. 1. Snapshot of a Si-n/p doped preform's fabricating process.

After the deposition of a porous un-sintered layer, sintering temperature is increased gradually from 1500 to 1800°C in the presence of gaseous mixture of 80% He and 20% $O_2$. Thereafter, the deposited tube is collapsed at high temperature (above 2000°C) for making a final optical preform.

Notice that Si-n/p concentration could be managed in the process through varying the flow rate of helium into the $SiCl_4$ bubbler as well as of Al vapor.

Finally, a Si-n/p doped fiber was drawn using a conventional fiber draw tower, applying the standard drawing technique. Notice here that the Si-n/p preform was annealed at around 1000°C for 4 hours with heating and cooling rate of 20°C/min into closed furnace before drawing of the fiber.

Worth noticing that a small amount of Ytterbium $(Yb^{3+})$ was embedded in the preform core (around 0.005 wt.%) for seeking an energy transfer between Si-n/p and $Yb^{3+}$ ions in the final Si-n/p doped fiber at excitation in or outside the resonant $Yb^{3+}$ band.

## III. Si-n/p Preform's Characterization

Refractive index (RI) profile of Si-n/p doped preforms was measured using a preform analyzer. In Fig. 2(a), we show the result of the RI profile measurement for the preform that was used to fabricate the Si-n/p fiber we further experimented. It is seen that the RI difference between the core and cladding areas of the preform is within a 0.006–0.007 range, allowing an estimate for numerical aperture (NA) to be made: $NA = 0.14$.

We also performed an electron probe micro-analysis (EPMA) of the fabricated preforms. An EPMA curve of the same Si-n/p fiber preform is demonstrated in Fig. 2(b). It is seen that the $Al_2O_3$ content in the preform core area is extremely small, ∼0.005–0.01 wt.% (the same holds for $Yb_2O_3$, see above), which is the minimum detection limit of the EPMA instrument. This result clearly indicates that the RI difference (see again Fig. 2(a)) was established in the preform due to the presence of Si-n/p, not Al or Yb (these species contribute in the RI difference at the level of $\sim 1 \ldots 2 \times 10^{-5}$). The presence of Si-enriched areas in core is confirmed by our measurements with the final Si-n/c fiber; see Section IV.

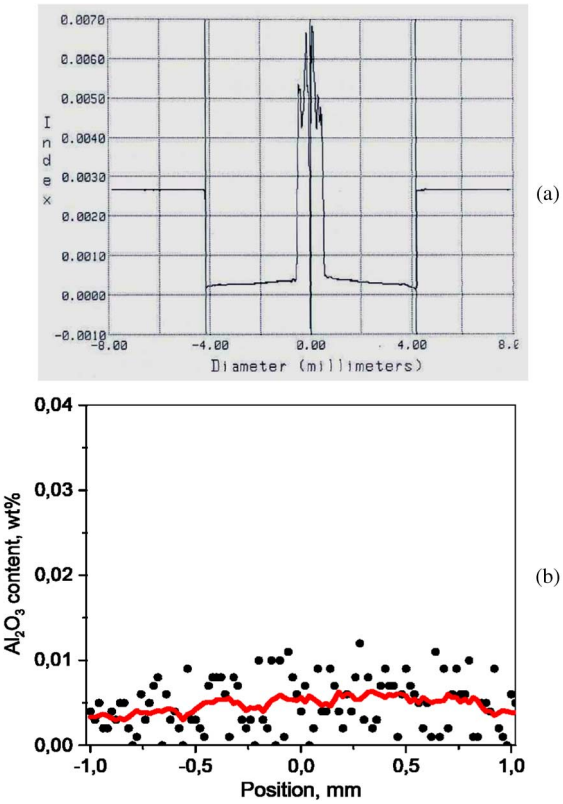


Fig. 2. (a) Refractive index profile of the Si-n/p doped preform and (b) $Al_2O_3$ distribution in the core area.

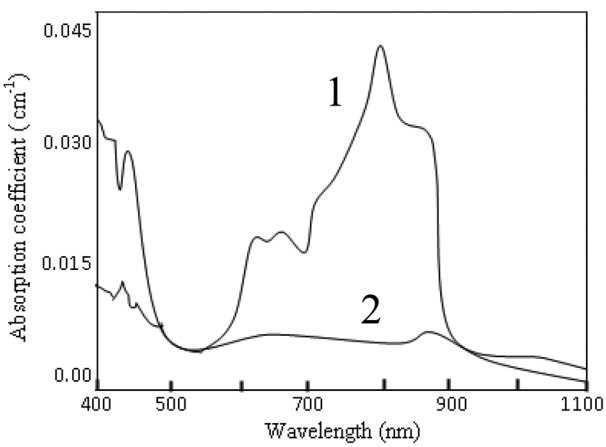


Fig. 3. Absorption spectra of the Si-n/p doped preform (curve1) and analogously made preform free from Si-n/p (curve 2).

Absorption spectra of the Si-n/p doped fiber preform were measured employing a monochromator and are shown in Fig. 3. The measurements were done using a modulated white-light source by guiding the light through a bundle fiber cable and focusing it onto the core region of the preform sample; the white-light beam was passed through the monochromator before being launched into the sample (notice that a pure silica glass sample of the same thickness as the preform sample was used as a reference). In turn, transmitted light was collected, through another bundle fiber cable, onto a Silicon photo-detector. The transmittance spectrum (measured within the wavelength range 400–1100 nm) was converted, using analyzing software, into the absorption spectrum.

From Fig. 3, where the Si-n/p preform absorption spectrum is demonstrated (see curve 1), it is seen a wide absorption band formed in the preform core region, which covers the wavelengths interval spanning from ∼550 to ∼900 nm. From the literature on Si-n/p based materials (see e.g. [17]–[19]), we can assign this spectrum as belonging to mainly amorphous Si n/p ($a$-Si). Thus, the production of crystalline Si-n/p phase(s) ($c$-Si) at the preform stage seems to be questionable since the absorption spectra of $c$-Si n/p have different character, viz., they should demonstrate a smooth dependence against wavelength, with absorption magnitude strongly rising towards short wavelengths and slope being defined by a characteristic size of $c$-Si n/p.

In Fig. 3, we also give an absorption spectrum of a preform fabricated in a similar way but without doping with Si-n/p (see curve 2). It is seen that in this case no pronounceable absorption features within the 550–900-nm range which could be related to Si-n/p are present. So the broad absorption band seen in the upper curve is justified to arise due to the presence of Si-n/p. In the meantime it deserves attention that both curves in Fig. 3 have the absorption bands spanned from UV to ∼500 nm, which most probably stem from the presence in both fibers of silica-related defect centers. Such centers (or "point defects") are known to be generated from imperfections of the $SiO_4$ continuous network, including the oxygen and silicon vacancies. Several types of such defects are known for silica fibers: surface E′-centers, self-trapped excitons, non-bridging oxygen-hole centers, neutral oxygen deficient centers, two-fold coordinated silicon lone-pair centers as well as hydrogen-related species and interstitial $O_2$-molecules. In our case, *in-situ* generated Si-n/p are embedded into the silica glass matrix under highly inert atmosphere, which may create Si-oxygen deficient centers and non-bridging oxygen-hole centers, generally showing absorption peaks within the UV-VIS region. An increased attenuation in these (400 to 500 nm) peaks in the Si-n/p doped preform as compared to the preform without Si-n/p (Fig. 3) indicates that the nanoparticles can be themselves a source of extra defect centers in silica glass.

The existence of Si-n/p in the fabricated preforms was verified by TEM measurements. The result of the TEM experiment with the Si-n/p preform is given in main frame of Fig. 4(a), from where we reveal that, within the Si-rich core region, Si-n/p with a diameter of 5–10 nm are formed. Furthermore, an inset in Fig. 4(a), which demonstrates an electron diffraction pattern obtained from the same preform sample, allows one to conclude on whether Si-n/p, at the preform stage, are amorphous or crystalline. From the inset it is seen that the above revealed hypothesis about the amorphous nature of Si-n/p in the Si-n/p doped preform is confirmed; indeed, the electron diffraction pattern does not show any diffraction pattern ring. On the other hand, the Raman spectrum of the same Si-n/p doped preform, which is shown in Fig. 4(b), demonstrates a very broad and smooth peak at 480 $cm^{-1}$ relatively to the probe laser line being 514 nm (an Argon laser) in our experiments. Both the peak's spectral position and shape signify the presence of Si in the amorphous phase at the Si-n/p preform stage. [In the meantime notice that after drawing fiber from this preform the situation regarding the

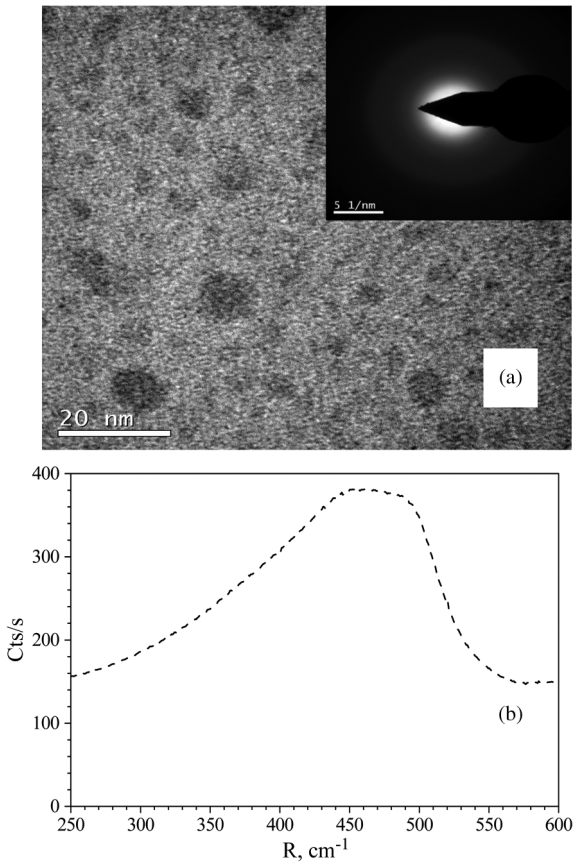


Fig. 4. TEM image (main frame) and electron diffraction pattern (inset) of the core region of the Si-n/p doped preform (a); Raman spectrum recorded for the Si-n/p preform (b).

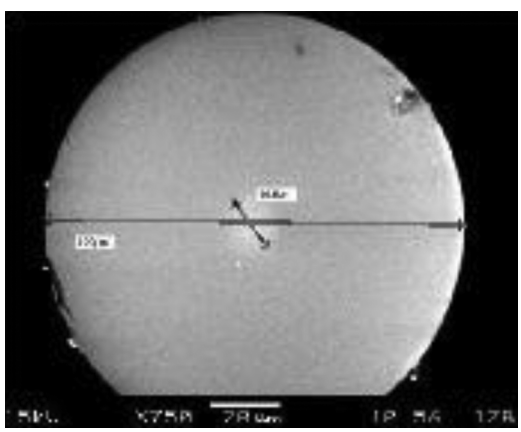

Fig. 5. Image of the Si-n/p fiber's cleaved end (obtained with an electron microscope).

absorption and Raman spectra, diffraction pattern, and other parameters is significantly changed; see Section IV].

## IV. Final Si-n/p Fiber's Characterization

### *A. Morphological Properties*

An image of the Si-n/p fiber drawn from the preform is shown in Fig. 5. It was obtained using an electron microscope with sub-$\mu$m resolution. It is seen that the Si-n/p fiber has outer diameter of 122 $\mu$m and the core diameter of 16 $\mu$m.

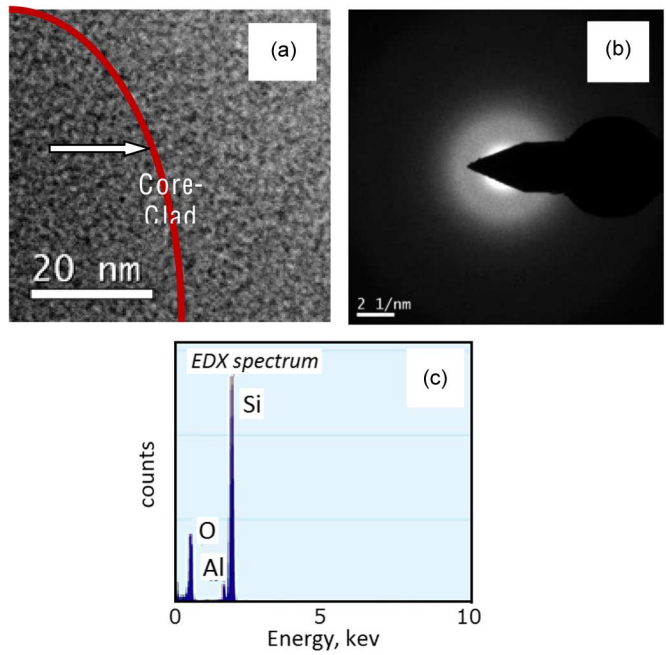


Fig. 6. (a) TEM image, (b) electron diffraction pattern, and (c) EDX spectrum taken from the core area of the Si-n/p fiber.

In order to confirm that after drawing the preform Si-n/p are kept within the fiber core, we have fulfilled a set of experiments, allowing insight into the morphological properties of the fiber.

A TEM image of the fiber's core region was obtained, which demonstrates (see Fig. 6(a)) the presence of small nanoparticles with an average size measured by a few nm only, thus being less in size than the particles at the preform stage. One of the reasons for decreasing the size of Si-n/p may be that the agglomerated particles, generated under the thermal annealing process, became non-agglomerated during the fiber drawing stage at a 30 g drawing tension at $\sim 2000^{\circ}$C.

Furthermore, it can be seen from the TEM picture that the nanoparticles in the Si-n/p fiber are slightly non-circular shaped and that most of them are situated near to the core clad-boundary (see the marked region in Fig. 6(a). Thus, it can be thought that Si-n/p, after drawing, become concentrated at the core-clad boundary, forming wires or droplets' strips.

Another point to be mentioned is that the Si-n/p preform was annealed before drawing the fiber. At the annealing stage, most of the amorphous Si-n/p could be converted to the crystalline ones (not at the fiber's drawing); however, it seems that at the drawing stage most of the crystalline Si-n/p diffused into the core-clad boundary.

In turn, the electron diffraction pattern obtained from the Si-n/p fiber core area shows that the particles are partially crystalline in nature: See Fig. 6(b) demonstrating diffraction rings attributable to polycrystalline nano-objects. This indicates notable transformations in the morphology of the core glass at drawing the fiber from the preform (remind that the nature of Si-n/p at the preform stage was entirely amorphous; refer to Fig. 4), with a possible reason being rather low crystallization temperature of Si-n/p [20].

We also made an EDX analysis in spots inside and outside the core region of the fiber. The EDX spectra taken from the area

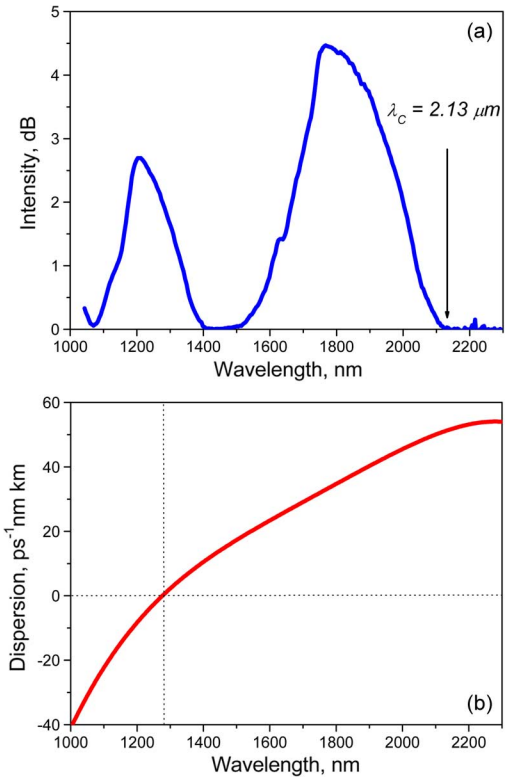


Fig. 7. (a) Relative transmission of the Si-n/p fiber in straight and coiled positions, revealing the cutoff spectral position (marked by arrow), and (b) the Si-n/p fiber's dispersion curve.

inside the core indicate that the particles are mostly Si-rich ones: Their local structure "embedded" into the core area is characterized by a much stronger signal corresponding to Si as compared with signals corresponding to Al and O (see Fig. 6(c)). Notice that the signals from Si, Al, and O obtained from the clad area of the fiber were "conventional", i.e. there was no prevalence of the signal from Si species over the ones from Al and O.

### *B. Wave-Guiding Properties*

The wave-guiding properties of the Si-n/p fiber were inspected applying the conventional procedures that allow insight to the modal and dispersive essences of the fiber. The results are shown in Fig. 7.

Fig. 7(a) demonstrates the experimental result revealing the cutoff wavelength of the Si-n/c doped fiber. The experiment comprised the standard procedure of measurements of the fiber attenuations placed straight and coiled over a small diameter. After proper processing the data obtained, an oscillating dependence of relative intensity in the wavelengths domain was built, which is shown in Fig. 7(a). The oscillations' stop wavelength (at about 2.13 $\mu$m) points out the sought cutoff wavelength of the fiber.

This result, together with the data on the value of Si-n/p fiber core diameter (Fig. 5), allowed us to determine NA of the fiber in the step-index approximation $(\mathrm{NA} = 0.11)$ and RI difference $(\Delta \mathrm{n} = 0.0043)$. Thus, the fiber's parameters are slightly different from those obtained for the preform from which the fiber originated.

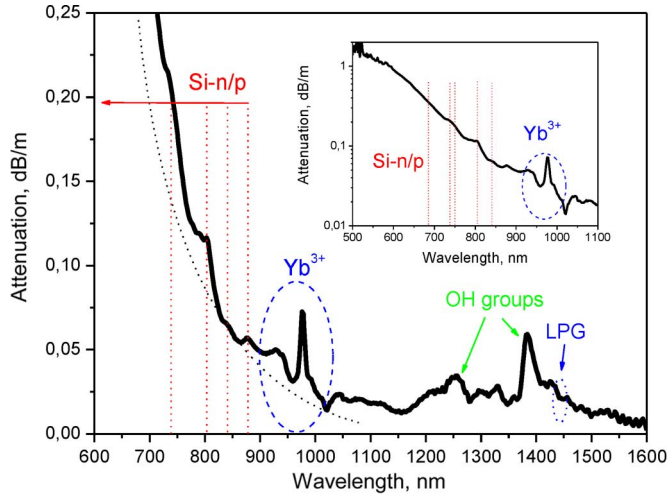


Fig. 8. Attenuation spectrum of the Si-n/p fiber; inset features rise of attenuation, ascribed to Si-n/p, towards shorter wavelengths (other details are featured in the text).

As for us, this difference is noticeable as being obviously connected with certain phase transformations in the core glass, which occur at drawing the fiber. We think that Si contained in the core region changes its state from entirely amorphous (see Figs. 3 and 4 in Section III) to at least in-partial crystalline phase because of the high temperature of the drawing process (it is well-known that the refractive index of amorphous silicon is greater than that of crystalline silicon). Some other evidences for such a scenario to happen are presented below.

Fig. 7(b) demonstrates the other wave-guiding property of the Si-n/p fiber, viz., its wavelength-dependent dispersion obtained using also a standard technique. It is seen that the fiber zero dispersion wavelength is near 1.3 $\mu$m, being compatible with conventional telecommunication fibers widely used in practice. The presented data are worthy for understanding the results to be presented below, which reveal the nonlinear properties of the Si-n/p fiber.

### *C. Optical Loss Spectra*

Fig. 8 (main frame) provides a view on the absorptive (loss) properties of the Si-n/p fiber. The loss spectrum was measured applying standard cutback measurements, using a white-light fibered source and an optical spectrum analyzer (OSA).

It is seen from the figure that the fiber demonstrates strong attenuation in the near-IR to VIS range. The main features here are a drastic increase of attenuation towards shorter wavelengths, which is a manifestation of the presence of Si-n/p in the form of $c$-Si in $SiO_2$ matrix [17], [19], [21], [22], and occurrence, at the same time, of several characteristic absorption peaks in VIS, which coincide in spectral positions with the ones presented in the absorption spectrum of the source Si-n/p fiber preform (Fig. 3). The last fact is in favor of that $a$-Si n/p be present in the fiber core.

The other features that deserve noticing are the presence of OH-groups peaks (at 1250 and 1380 nm) [7] and $Yb^{3+}$ resonant-absorption band within a 900–1100 nm range. We can also propose that considerable rise of loss towards shorter wavelengths (see inset to Fig. 8) is at least partially associated

with the presence of scattering, an inevitable factor given by the presence of nano-scale range inclusions (Si-n/p) in the fiber's core.

### *D. Raman Spectra*

We measured Raman response of the Si-n/p fiber, employing the standard technique [19] adapted to optical fibers. We found necessary to compare it with the Raman signals from a standard telecom fiber (SMF-28) and analogous fiber with purely $SiO_2$-based core in order to deduce a contribution in the Raman signal stemming from the presence of nanoparticles in the core area of our Si-n/p fiber. [Notice that as SMF-28 fibers also contain Germanium in core, which contributes in the Raman signal, the use of purely $SiO_2$-based fiber for the comparison needs was essential for making conclusions].

We also measured Raman response from bulk (amorphous, poly-, and mono-crystalline) Si samples. The excitation wavelength in all cases was, as in the case of Raman studies with the Si-n/p preform (Fig. 4), 514 nm. The results are presented in Fig. 9.

Fig. 9(a) demonstrates the Raman spectrum of the Si-n/p (curve 1) fiber together with the ones of SMF-28 (curve 2) and $SiO_2$-based (curve 2′) fibers. The two important points stem from the figure: (*i*) the Si-n/p fiber demonstrates rather strong fluorescence seen as a plateau (dotted line) at which the detected signal approaches at larger wave numbers (about the fluorescence details—see below); (*ii*) the Si-n/p fiber has certain well-detectable features nearby the main peak of the Raman signal (at wave numbers 300–700 $\mathrm{cm}^{-1}$).

After normalization of all the spectra shown in Fig. 9(a) (they were obtained at using different fibers' lengths) and then subtracting each of the last two spectra from the former (for the Si-n/p fiber), we obtained the differential Raman spectra shown in Fig. 9(b) as curves 2 and 2′, which are supposed to shed more light on the features given by "net" contribution of Si-n/p in the Si-n/p fiber.

A few well-pronounced peaks are seen in the differential spectrum, which are located at around 310, 470, and 510 nm and can be related to the ones known both for $a$-Si and $c$-Si n/p, being superimposed [23]–[32]. It is interesting to compare this spectrum with the ones presented in Fig. 9(c) and (d), where we plot the Raman signals measured in a separate experiment where we dealt with amorphous, polycrystalline, and single-crystalline bulk Si samples (c) and also with bulk samples containing Si nano-crystallites of different types (d). One can notice, from the direct comparison of the results (b), (c), and (d), that the Si-n/p fiber demonstrates an averagely smaller contribution of $c$-Si signal on the background of $a$-Si signal. This seems to be in agreement with the analysis of the attenuation spectra of the Si-n/p fiber (Fig. 8), where we argued about the same matter by noticing the behavior of the fiber's losses that tailor to shorter wavelengths.

A reliable conclusion on what could be weight percentages of $a$-Si and $c$-Si n/p in the core region of the Si-n/p fiber cannot be made from these experiments, whereas the part of the Raman signal ascribed by us to the presence of Si—can: It is measured by ∼25%. Thus, it is worth to conclude that the core area of the

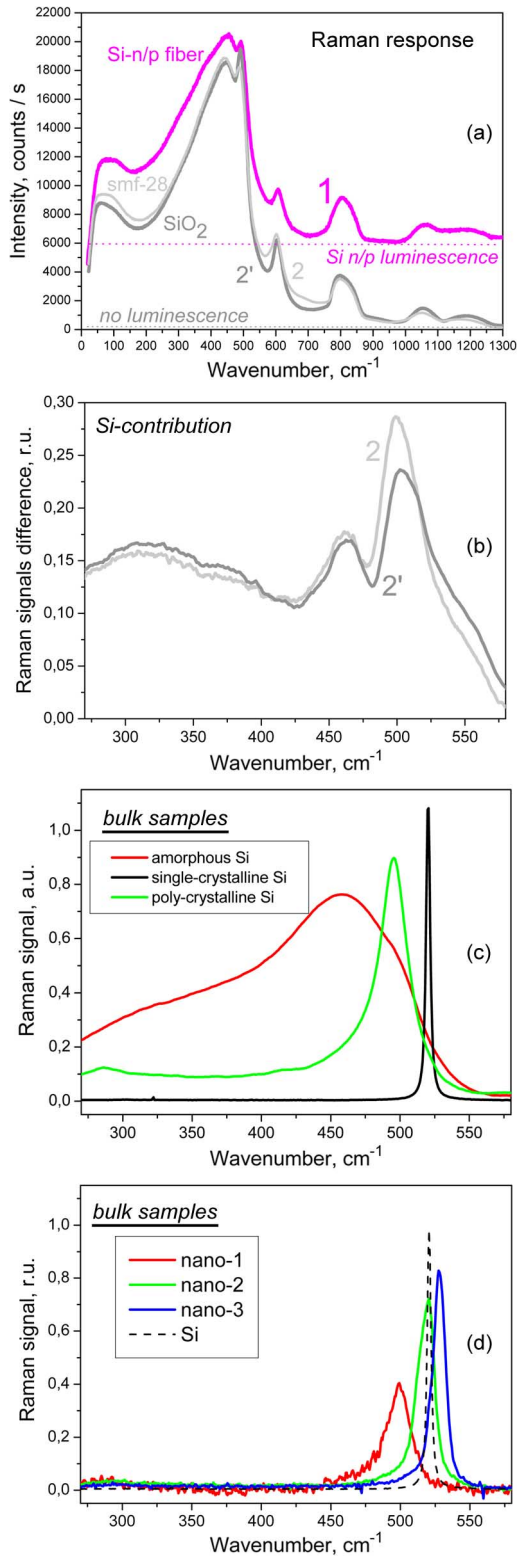


Fig. 9. (a) Raman spectra recorded for the Si-n/p and Si-free fibers; (b) these spectra' difference ascribed to a net Si-n/p contribution, (c) Raman spectra obtained for bulk samples doped with different-kind n/p, and (d) Raman spectra of amorphous, single- and poly-crystalline bulk Si.

Si-n/p fiber became, in any case, kept strongly enriched with Si after drawing the fiber from the preform while the nature of this extra Si is nano-sized (polycrystalline) Si-n/p, thus confirming the above made conclusion on the morphology of the core glass,

which was revealed from the TEM, EDX, and electron-diffraction analyses for the fiber; see Fig. 6.

It also deserves attention a direct comparison of the Raman spectra obtained from the Si-n/p preform from which the Si-n/p fiber has been drawn (Fig. 4(b)) and the reference bulk one (Fig. 9(c)), which look almost equal. Thus, it becomes confirmed the above proposed hypothesis on the change of the nanoparticles, from amorphous ($a$-Si) to partially crystalline ($c$-Si) phase after drawing the fiber from the preform.

### *E. Fluorescence Spectra*

In Figs. 10–14, we demonstrate the fluorescence spectra of the Si-n/p fiber after excitation at 406, 633, and 978 nm wavelengths.

First, a semiconductor laser oscillating in CW regime at 406 nm (70 mW) was employed to pump the Si-n/p fiber; pump light was launched into the fiber using a collimator. Fluorescence spectra were collected from another fiber side; the output radiation was delivered to the OSA using a multimode patch-cord. In order to get the Si-n/p fluorescence dependence upon the pump power, we attenuated the pump light by placing neutral filters between the laser output and the collimator. We were interested in response of Si-n/p, when they are excited far from the main absorption bands that are usually thought to belong to $a$-Si (see Fig. 3), implying that the 406 nm pump can only excite nanoparticles being in $c$-Si phase (see Fig. 8). Note that pump intensity in the fiber core reached the value of $\sim 2.5\ \mathrm{kW/cm^2}$.

The results of the measurements obtained for the Si-n/p fiber lengths of 4.5 and 17.5 m are presented in Fig. 10(a) and (b), respectively. For comparison, we have also made similar measurements for a standard 17-m Si-free multimode fiber in the same arrangement; see Fig. 10(c). Insets to Fig. 10(a)–(c) provide the values of pump power at the fibers entrance.

Note that besides the pump remnant at 406 nm and the pump ripples at 812 and 1218 nm, which originate from the OSA internal gratings (marked by arrows), a few pronounced fluorescence bands, spanned from 500 to 1600 nm, are present in the spectra of the Si-n/p fiber (Fig. 10(a), (b)), but not—in the spectrum of the Si-free multimode fiber (Fig. 10 (c)). Evidently, the wide spectral bands in Fig. 10(a) and (b) should be attributed to Si-n/p.

The shape of Si-n/p-related fluorescence spectrum has a very interesting character. Instead of a smooth fluorescence band centered at approximately 800 nm, reported in many previous works, in our case the spectral response of Si-n/p is composed of at least four bands. Hereafter we label these bands as "I" for the peak centered at 650, "II" at 950, "III" at 1230, and "IV" at 1540 nm (the peak at 800 nm is weak). The bands I—IV can be compared to the ones found in the work [33] where authors ascribe such bands to Si-n/p as being in different phases. For us the most intriguing fact is multi-peak structure of the bands; such multi-peak structuration is clearly seen within the bands I and II but it can be also captured—with a higher OSA sensitivity—within the band III. We suppose that the physics that would stand behind the multi-peak structure of the fluorescence bands should involve the phonon spectra of $SiO_2$ matrix and Si n/p, which would spectrally "modulate" the detected fluorescence [33]–[37]. In turn, the appearance

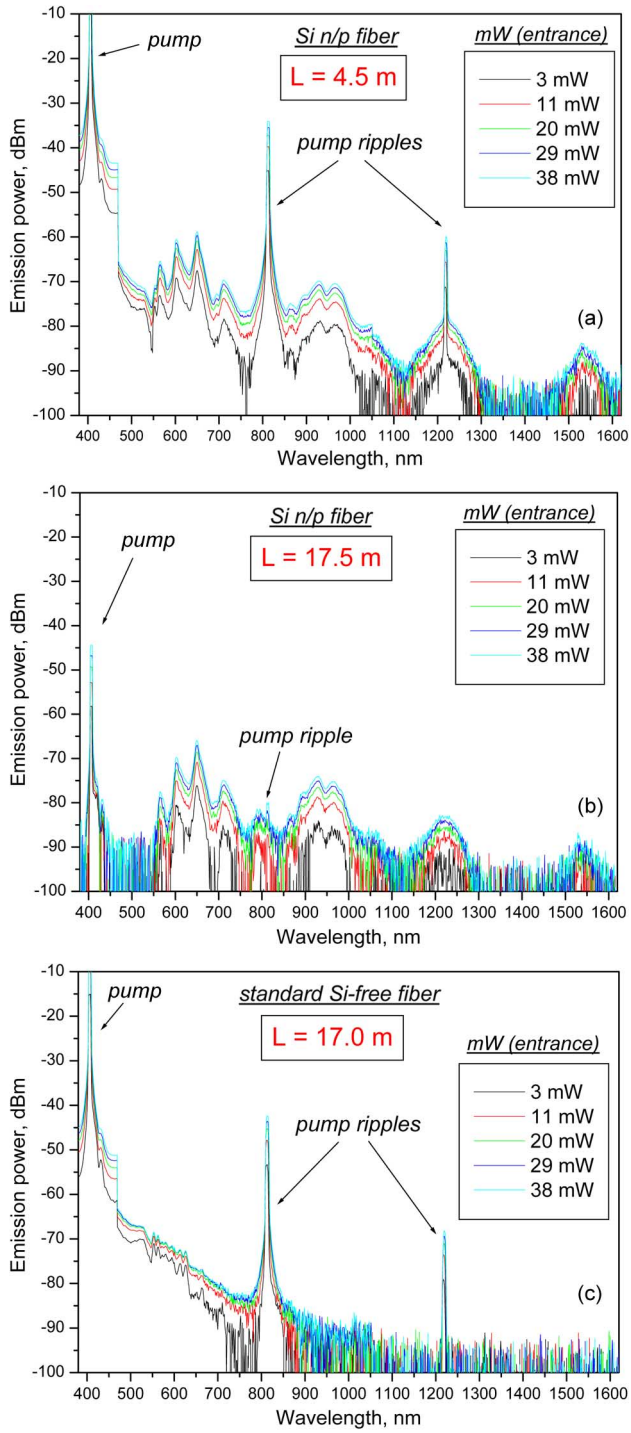


Fig. 10. Fluorescence spectra obtained at 406-nm excitation from the Si-n/p fiber for (a) 4.5 and (b) 17.5 m lengths and from the Si-free fiber (c). Insets show pump powers @406 nm launched to the fibers.

of the spectrally segregated bands, from I to IV, might itself stem from a resonant coupling of sub-systems of Si n/p and $SiO_2$ where Si-n/p of a definitive size are excited through the assistance of phonons having definite energies. We shall discuss the $\mathrm{Si-n/p'}$ fluorescence features in more details elsewhere.

As a natural continuation of the data reported in Fig. 10, in Fig. 11(a) we present the energy diagram obtained after formal re-calculating the wavelengths, corresponding to each band (from I to IV) in Fig. 10(a), (b), into the energies' domain. We

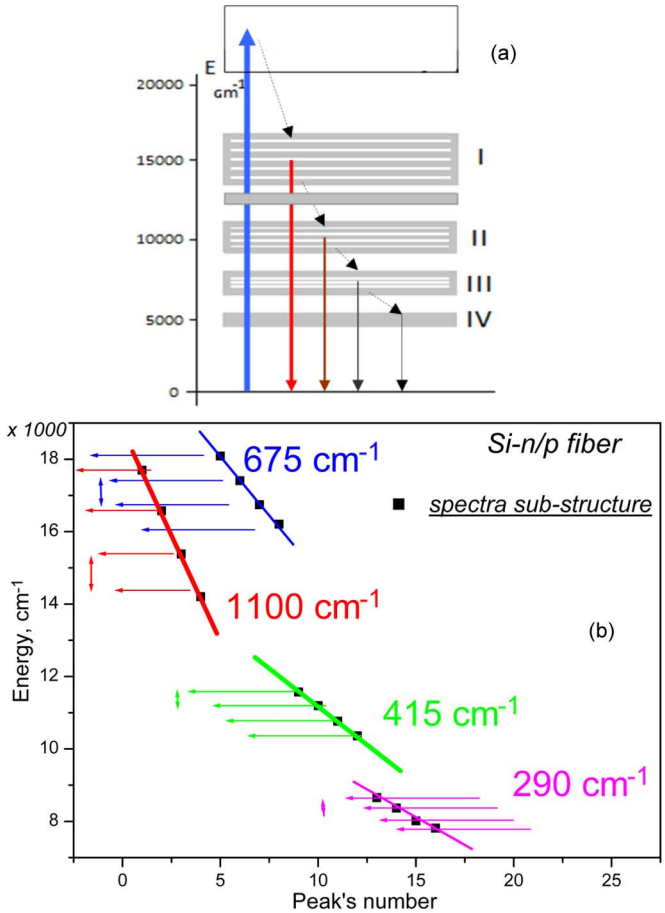


Fig. 11. (a) Energy diagrams for the bands I to IV (a) and for their multi-peak spectral structures (b), deduced from the spectra (a) and (b) shown in Fig. 10.

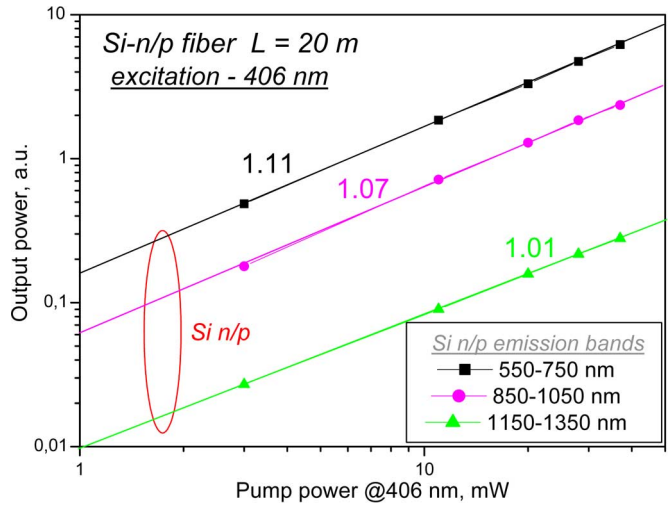


Fig. 12. Log-log dependences of integrated output powers within the bands I to III (see inset) on pump power @406 nm.

also present, see Fig. 11(b), the results of such re-calculation for the sub-peaks in the multi-peak structures of the bands I to III. Each point in the diagram shown in Fig. 11(b) corresponds to the position of sub-peaks from the left to the right side throughout the spectra: Numbers 1 to 8 are associated to the sub-peaks located within band I, numbers 9 to 12 are associated to the sub-peaks within band II, and numbers 13 to 16—for the less resolved band III (band IV at 1540 nm could not be treated as the previous ones because of the absence in it of such structure). The most important conclusion from Fig. 11(b) is that the sub-peaks within the bands I to III are almost equidistant: See the lines of different colors in the figure, which are included as a guide to the eye.

The most prominent sub-peaks (within the band I) are separated by around 1100 and 415 $\mathrm{cm}^{-1}$. It is known from the literature on silica fibers (see e.g. [25], [38]) and it also follows from Fig. 9(a) (where we report the Raman signal of the Si-n/p fiber), that these values correspond to $SiO_2$ phonon energies. In this way our earlier statement regarding the role of the phonon spectrum in producing the spectrally "spiked" fluorescence of the Si n/p fiber is confirmed. This leads us to conjecture that the Si-n/p fluorescence is assisted by the flow of energy from $SiO_2$ phonons, i.e. that the real sources of fluorescence being the areas at the interface of Si n/p and $SiO_2$ (such ideas have been extensively developed in the literature on nano-sized Si in silica; see e.g. [1], [30], [39]–[46]). Other spectral intervals, 675 and 290 $\mathrm{cm}^{-1}$ (Fig. 11(b)) can be associated in a similar way: These values can be related to the phonon spectrum of Si nuclei of a Si n/p, say, to the 2TA and LA acoustic phonon mode (295 $\mathrm{cm}^{-1}$). However a more detailed experimental study is apparently needed for confirming the ideas.

Regarding the bands' energy diagram shown in Fig. 11(a), no reliable conclusion on what is their origin can be made at the present stage of our knowledge. We only propose that such fluorescence band structure could be an appearance of small-size (sub-nanometer) emitting objects, say, interfaces of Si-n/p with $SiO_2$ matrix (refer again to [1], [30], [39]–[47]), but not of Si-n/p (their cores) themselves. Or, alternatively, these bands can be ascribed to some defect centers formed at the fiber drawing (see e.g. [47]–[50]), say, to non-bridging oxygen-hole centers, which fluoresce either after direct excitation at 406 nm or as a result of energy transfer from the excited Si-n/p (whose "normal" weak fluorescence is seen nearby 800 nm; Fig. 10(b)).

Further information is contained in the integrated powers within the fluorescence bands. Here we report the integrated powers of bands I to III as functions of pump power (see Fig. 12); notice that we plot in the figure the data in a log-log scale where the inset specifies each of the curves.

One can see that the integrated fluorescence power, in each of the spectral bands reported, follows a super-linear law; that is, the slopes of the dependences exceed 1. This behavior indicates a negligible saturating effect within the available pump range and net positive gain in the fiber. This is an interesting result since it points to the potential use of the fabricated Si-n/p fiber for laser or amplifying applications [1], [18], [51].

The fluorescence data obtained for the Si-n/p fiber at 406-nm excitation is supported by a photo in Fig. 13, which shows the fluorescence of the fiber in these pump conditions. The light from the lateral surface of the fiber is seen to be in the VIS region, with a maximal emissivity to be in the red spectral range. Unfortunately, power of the lateral emission was too weak to be recorded using our OSA; for that reason it was not possible to make a direct comparison of the fluorescence spectra in the lateral and frontal (see Fig. 10) detecting configurations.

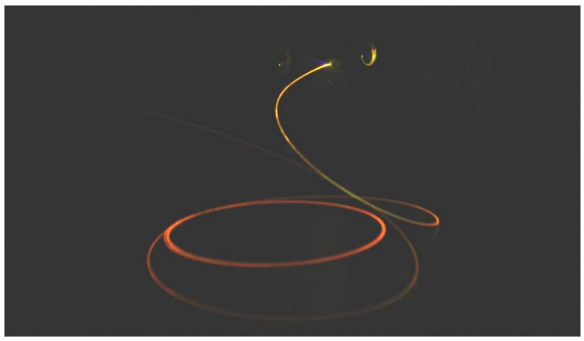

Fig. 13. Photo of the Si-n/p fiber fluorescence under excitation by 50 mW at 406 nm.

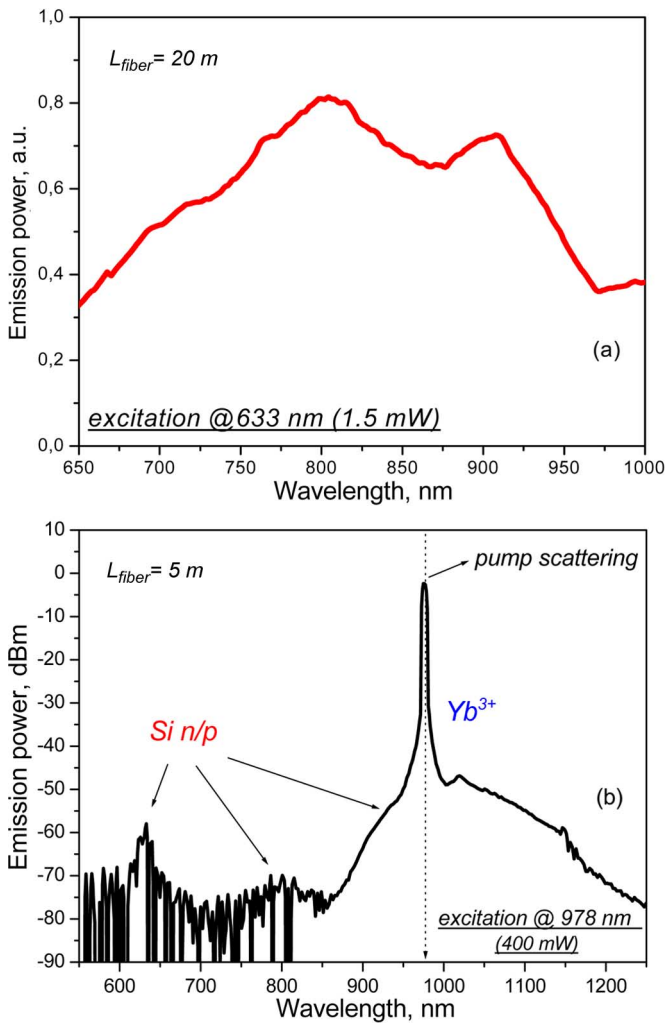


Fig. 14. Fluorescence spectra obtained at (a) 633 and (b) 978 nm excitation from the Si-n/p fiber.

From Fig. 13, we also observe that in places where the fiber is deformed the fluorescence spectrum is a bit modified, one of explanations of which could be influence of intra-fiber stresses upon the Si-n/p local structure "embedded" within the $SiO_2$ matrix.

We now turn to Fig. 14 where we show the data on the fluorescent properties of the same Si-n/p fiber when it is pumped at 633 nm (a He/Ne laser, 3 mW; Fig. 14(a)) and 978 nm (a diode laser with a fiber output and power of 400 mW; Fig. 14(b)).

In both cases, a setup was such that the fluorescence spectra were measured from the fiber's side, opposite to the pump light launching. In this way the background offset of the measured spectra was diminished. Notice that a standard focusing scheme using an objective (X20) was employed in the first case (for coupling light @633 nm from the He/Ne laser, with coupling efficiency of around 40%) and an all-fiber arrangement that involved an isolator and WDM multiplexor—in the second case (for launching light @978 nm from the diode laser). In both experiments, rather long pieces of the Si-n/p fiber were used (20 and 5 m, respectively) to provide better signal-to-noise ratio in the spectra.

It is seen from Fig. 14(a) that, in spite of low power delivered (1.5 mW) by the He/Ne laser to the fiber, Si-n/p fluorescence in VIS is well detectable and bands I and II can be segregated at the slopes of an 800-nm maximum. From Fig. 14(b), it is seen that similar features in Si-n/p fluorescence occur at 978-nm excitation, however at the Stokes side of the spectrum the $Yb^{3+}$ emission dominates (remind that the Si-n/p fiber was weakly doped with $Yb^{3+}$, see Fig. 8). It is important to remark that, in the last case, the origin of the fluorescence bands in VIS is up-conversion, since they are located at the anti-Stokes side of the excitation wavelength. This observation could be a direct justification for the existence of an energy transfer process from the excited $Yb^{3+}$ ions to Si-n/p, a phenomenon not observed in the existing literature. On the other hand, the reverse process (energy transfer from Si-n/p to $Yb^{3+}$ at 406-nm excitation, see Fig. 10) was not observed, probably because of low Si-n/p concentration in the fiber. The other spectral bands, III and IV, seen in Fig. 10 (obtained at 406-nm excitation) were not clearly detected under low-power 633-nm excitation (the He/Ne laser) whereas we were unable to resolve them under moderated-power 978-nm excitation, in this case because of the presence of $Yb^{3+}$ fluorescence in the near-IR region.

### *F. Nonlinear-Optical Properties*

The results of experiments from which we estimated the nonlinear RI change in the Si-n/p doped fiber are presented in Figs. 15 and 16. The motivation to conduct these experiments is promising applications of the nonlinear-optical properties of the Si-n/p fiber (see e.g. Section V).

There are different approaches to estimate the RI nonlinearity. We have chosen the most reliable and at the same time simple method [52], where the fiber under study is placed between a couple of long-period fiber gratings (LPGs) forming a "modal" interferometer within a wavelength domain limited by tens of nm. We used the setup first proposed in [52] (see also Fig. 15(a)), so that the model developed by the authors in order to estimate the RI nonlinearity is applicable to our case. The interferometer is formed because the guided modes that propagate within the core region of the fiber under test interfere with the modes that partially escape (by the first LPG) and return (by the second LPG) to the core region; so these propagate partially in the clad region. Spectral fringes at the output of the second LPG are observed under low-power white light illumination. The fringes occur due to a wavelength-dependent

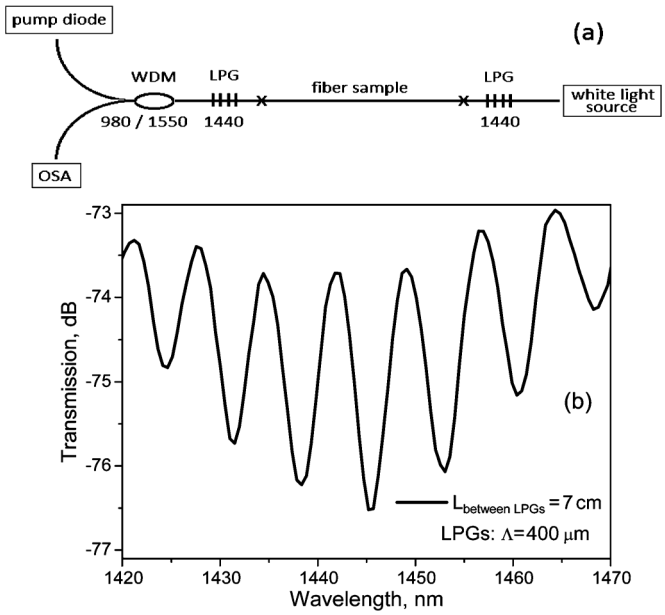


Fig. 15. (a) Interferometer optical scheme and (b) example of spectral interference of white light passed a couple of LPGs written in SMF-28 fiber.

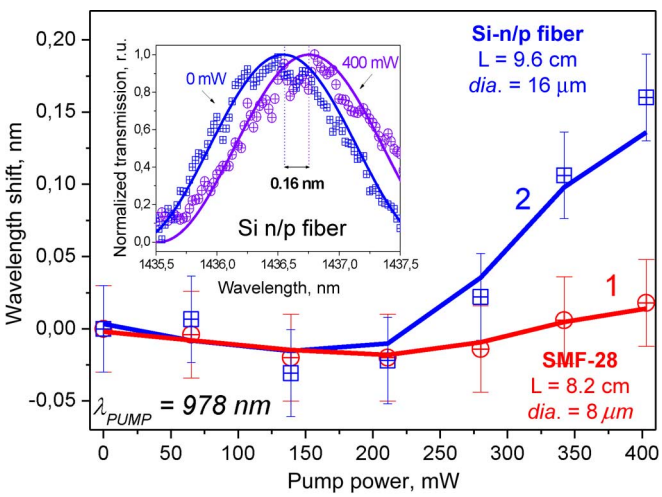


Fig. 16. Dependences of spectral shift in the SMF-28 (curve 1) and Si-n/p (curve 2) fibers versus pump power @978 nm. Inset shows how spectral fringes in the Si-n/p fiber are shifted at increasing the pump power.

phase difference between the mode propagating through the fiber core and the mode propagating partially through the fiber clad between the LPGs. Due to the nonlinear properties of the fiber placed between the LPGs, the RI of core of this fiber can be changed by launching high-intensity light into it. This will produce an additional phase change between the two interfering modes, which shifts the interferometer pattern. Thus, when the interferometer is pumped both with low-intensity white light and high-intensity pump (with wavelength out of the interferometer band), one will observe that the spectral position of the interference fringes is shifted as the whole. In this way the nonlinear part of the RI, $n_2$ ($\chi_{(3)}$ susceptibility) of the tested fiber's core can be measured.

The fringes' pattern shown in Fig. 15(b) was obtained when the fiber between the LPGs is the same as the one used to fabricate the gratings (SMF-28) with 400 $\mu$m space between the graves that form the gratings (the LPGs were expected to be optimal for 1.44 $\mu$m; see Fig. 8). The pattern shown in Fig. 15(b) was obtained with weak white light as a probe launched from one side of the interferometer and detected at the opposite side with the OSA. The semiconductor laser at 978-nm with the maximal output power of 500 mW pumps the fiber under test from the interferometer's opposite side where the white-light is launched. This was achieved by splicing a WDM multiplexor (980/1550 nm) with the interferometer.

The result of an experiment when an 8.2 cm piece of standard SMF-28 fiber was placed between the LPGs is shown by curve 1 in Fig. 16.

The result obtained from a similar experiment in which SMF-28 fiber was replaced with a piece of the Si-n/p fiber (length, 9.6 cm) is shown in the same figure by curve 2. An example of how the fringes' pattern, in the last case, suffers a spectral shift when the pump power at 978 nm is increased from 0 to 400 mW is presented in the inset to Fig. 16. Note that due to the multimode propagation regime at around 1.44 $\mu$m in the Si-n/p fiber (see Fig. 7(b)) the visibility of the interference pattern was significantly worse than that for the SMF-28 fiber (single-mode at this wavelength). However, this was not a serious obstacle to handle the experiment (see e.g. the inset in Fig. 16 where the normalized sinusoidal-like patterns of fringes are clearly seen).

One can note from Fig. 16 that the wavelength shift rises much faster in the Si-n/p fiber than in the SMF-28 when the pump power at 978-nm is increased. Furthermore, the maximal shift of the interference fringes detected for the Si-n/p fiber is about 5–10 times larger than the one for the SMF-28 fiber (at the maximal pump power). It should not be overlooked that the diameters of the fibers differ approximately by a factor of 2 (16 and 8 $\mu$m, respectively). Thus, the RI nonlinearity in the Si-n/p fiber is revealed to be notably higher than in SMF-28.

Using the parameters of the fibers given in Figs. 15 and 16 and assuming that the RI nonlinearity is mostly of the third-order for both fibers, we obtain the following estimates for the nonlinear RI: $n_{2(\mathrm{Si-n/p})} =\sim 5 \times 10^{-17}$ m$^2$/W and $n_{2(\mathrm{SMF-28})} < 5 \times 10^{-19}$ m$^2$/W. Notice that the $n_2$ value for the SMF-28 fiber is below the method's resolution (see curve 1 in Fig. 16) and therefore this estimate is not trusty. On the other hand, the $n_2$ value for the Si-n/p fiber is reliable, at least roughly (see curve 2 in Fig. 16). Our estimation is in agreement with the independently determined $n_2$ values for other Si doped fibers [7], [12]. It should not be forgotten that the estimate for $n_2$ for our Si-n/p fiber was made for 1.44 $\mu$m wavelength, whereas the nonlinear RI was "created" at the wavelength 978 nm. The resonant absorption at 978 nm ($\mathrm{Yb}^{3+}$) as well as the absorption tail given by Si-n/p, both being quite small (less than 0.1 dB/m; see Fig. 8), are expected to be harmless for the obtained $n_2$ value.

It is worth remarking that even if the method we used can provide a rough estimate of $n_2$, our results clearly demonstrate that the nonlinear RI of the Si-n/p fiber is significantly higher than that of the Si-free fiber. In future we plan to consider fibers with

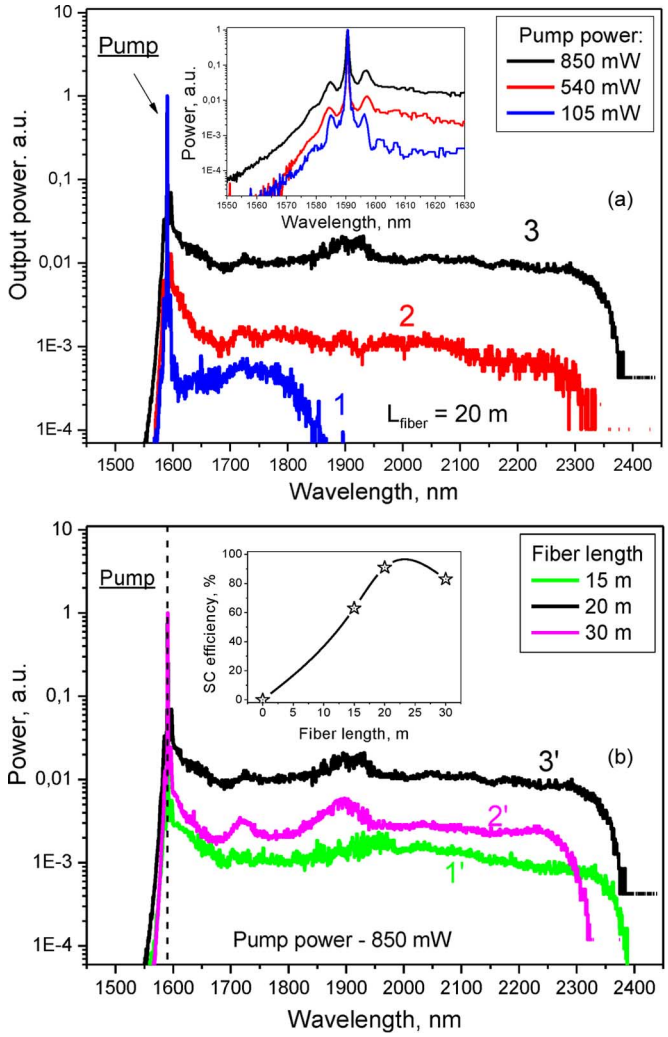


Fig. 17. SC spectra obtained from the Si-n/p fiber at 1.59 $\mu$m excitation (details are featured in the text).

a smaller core region and higher content of Si n/p, in attempt of getting stronger nonlinearities.

## V. Application: Supercontinuum Generation

A demonstration of the high nonlinear properties of the Si-n/p fiber is the effective supercontinuum (SC) generation when the fiber is pumped by a train of short (35 ns) powerful(up to 5.5 kW) pulses with maximal energy of 0.2 $\mu$J. The pulses are delivered by a double-clad Erbium doped fiber laser (EDFL, wavelength, 1.59 $\mu$m), oscillating in a passive Q-switch regime using a Thulium doped fiber [53]. Average output power of the EDFL was 0.95 W and the repetition rate of pulsing (kHz-range) was dependent on pump power. Output of the EDFL was spliced to the Si-n/p fiber through a fibered isolator.

Fig. 17 illustrates the optical spectra at the output of the Si-n/p fiber.

In Fig. 17(a), we present the output spectra of the Si-n/p fiber obtained at different pump powers but fixed length of the fiber (curves 1–3), while Fig. 17(b) shows the spectra obtained at different lengths of the fiber but fixed pump power (curves 1′–3′). It is seen that the output radiation presents an almost structureless SC expanded from the pump wavelength mostly to the Stokes side; the flatness of SC is remarkable, especially at the optimal conditions corresponding to the maximal pump power launched into the Si-n/p fiber (the average power is 850 mW) and its length of about 20 m.

Worth remarking is that several smooth and wide components, corresponding to the stimulated Raman scattering (SRS), are distinguishable in the spectra. Seemingly, this means that the SC generation is formed by the SRS cascade process (in the anomalous dispersion region of the Si-n/p fiber, see Fig. 7(a)). On the other hand, in the vicinity of pump wavelengths where SC starts, the characteristic spectral oscillations at both Stokes and anti-Stokes sides develop (see the inset in Fig. 17(a)). This may mean that a starting mechanism for SC generation is the offset of modulation instability and self-phase modulation, with the spectral oscillations on sidebands of the pump (1.59 $\mu$m) wavelength being enhanced by the pump, thus spreading the pulse spectrum aside. This process is then boosted up by the Raman response in the fiber.

The SC extends over the whole transparency region of the fiber, with its red and blue bounds to happen due to a significant increase of attenuation in the fiber because of the presence of OH-groups (see Fig. 8) (anti-Stokes side, $< 1.5$ $\mu$m) and silica matrix absorption (Stokes side, $> 2.4$ $\mu$m).

Finally, note the high efficiency of SC generation in the Si-n/p fiber. The inset in Fig. 17(b) shows that up to 93% of output power from the Si-n/p fiber is contained in SC (at approximately 20-m length of the fiber and maximal pump power, 850 mW); the overall SC power at the exit of the fiber was measured to be 420 mW. To the best of our knowledge, the reported result on SC generation in Si-n/p fiber is the first demonstration of such kind of effect (so far, SC generation in a Si-nanowire doped waveguide was reported only [54]).

## VI. Conclusions

The fabrication of a new-type Si-n/p doped fiber entirely based upon the MCVD process is reported. The formation of Si-n/p, at the preform stage and preservation at the fiber stage, is confirmed by the TEM, EPMA, EDX, electron diffraction, Raman, optical absorption, and fluorescence spectra measurements. The results reported in this work reveal that: (*i*) the wave-guiding properties of the fiber are due to excess of Si in the core region; (*ii*) the phase of Si-n/p is changed from mostly amorphous to partly crystalline after drawing the fiber from the preform; (*iii*) the fiber is fluorescence-active due to the presence of Si-n/p; (*iv*) the fluorescence has a multi-peak spectral structure within a few wide bands in the VIS to near-IR spectral region, which is most probably connected with a strong interaction of Si-n/p with $SiO_2$ matrix; (*v*) a peculiar property of the fiber is energy transfer between $Yb^{3+}$ ions and Si-n/p; (*vi*) the Si-n/p fiber has a higher nonlinearity $n_2$ than conventional (Si-free) fibers. It is also shown that the high $n_2$ value makes this fiber an effective source of supercontinuum. In conclusion, the study performed in this work shows that Si-n/p fibers of such type can be of interest for diverse practical applications as well as in basic research, however further studies are necessary in order to enhance their properties and for deeper understanding of the physics behind their performance.

## ACKNOWLEDGMENT

The authors are thankful to Drs. A. Levchenko and L. Iskhakova (Fiber Optics Research Center, Moscow, Russia) for the help in making some of the experiments, to Dr. I. Torres-Gomez (CIO, Leon, Mexico) for providing LPGs, and to Drs. A. Kurkov, N. Il'ichev, N. Kononov (A.M. Prokhorov General Physics Institute, Moscow, Russia), and A. Timoshenko (M.V. Lomonosov Moscow State University, Moscow, Russia) for useful discussions. The co-authors also thanks to Mr. K. Dasgupta, the Acting director of CGCRI, for continuous encouragement, guidance and support.

## REFERENCES

[1] L. Pavesi, L. Dal Negro, C. Mazzoleni, G. Franzo, and F. Priolo, "Optical gain in silicon nanocrystals," *Nature*, vol. 408, pp. 440–444, 2000.

[2] D. Riabinina, C. Durand, F. Rosei, and M. Chaker, "Luminescent silicon nanostrauctures synthesized by laser ablation," *Phys. Stat. Sol.*, vol. 204, pp. 1623–1638, 2007.

[3] K. Kusova, O. Cibulka, K. Dohnalova, I. Pelant, J. Valenta, A. Fucikova, K. Zidek, J. Lang, J. Englich, P. Matejka, P. Stepanek, and S. Bakardjieva, "Brightly luminescent organically capped silicon nanocrystals fabricated at room temperature and atmospheric pressure," *ACS Nano*, vol. 4, pp. 4495–4504, 2010.

[4] S. Kim, D. H. Shin, D. Y. Shin, C. O. Kim, J. H. Park, S. B. Yang, S. Choi, S. J. Yoo, and J. G. Kim, "Luminescence properties of Si nanocrystals fabricated by ion beam sputtering and annealing," *J. Nanomater.*, vol. 2012, p. 572746, 2012.

[5] S. Furukawa and N. Matsumoto, "Effects of polysilane formation on the optical and electrical properties of binary Si:H alloys," *Phys. Rev. B*, vol. 31, pp. 2114–2120, 1985.

[6] N. Daldosso and L. Pavesi, *Nanosilicon*. New York, NY, USA: Elsevier, 2005, ch. 5.

[7] P. R. Watekar, S. Moon, A. Lin, S. Ju, and W. T. Han, "Linear and nonlinear optical properties of Si nanoparticles/Er-ions doped optical fiber," *J. Lightw. Technol.*, vol. 27, pp. 568–575, 2009.

[8] A. Martinez, S. Hernandez, P. Pellegrino, O. Jambois, B. Garrido, E. Jordana, and J. M. Fedeli, "Optical nonlinearities in Si-nanocrystals at 1064 nm excited by nanosecond-pulses," *J. Appl. Phys.*, vol. 108, p. 014311, 2010.

[9] G. P. Agrawal, "Nonlinear fiber optics: Its history and recent progress," *J, Opt. Soc. Amer. B*, vol. 28, pp. A1–A9, 2011.

[10] J. Toulouse, "Optical nonlinearities in fibers: Review, recent examples, systems applications," *J. Lightw. Technol.*, vol. 23, pp. 3625–3641, 2005.

[11] S. Moon, B. H. Kim, P. R. Watekar, and W. T. Han, "Fabrication and photoluminescence characteristics of $Er^{3+}$-doped optical fiber sensitized by Si particles," *J. Non-Crystall. Solids*, vol. 353, pp. 2949–2953, 2007.

[12] S. Moon, A. Lin, B. H. Kim, P. R. Watekar, and W. T. Han, "Linear and nonlinear optical properties of the optical fiber doped with silicon nano-particles," *J. Non-Crystall. Solids*, vol. 354, pp. 602–606, 2008.

[13] P. R. Watekar, S. Ju, and W. T. Han, "Visible-to-infrared down-conversion in the silicon nanoparticles-doped optical fiber," *Current Appl. Phys.*, vol. 9, pp. S182–S184, 2009.

[14] G. Brasse, C. Restoin, J. L. Auguste, S. Hautreux, J. M. Blondy, A. Lecomte, F. Sandoz, and C. Pedrido, "Nanoscaled optical fibre obtained by the sol-gel process in the $SiO_2 - ZrO_2$ system doped with rare earth ions," *Opt. Mater.*, vol. 31, pp. 765–768, 2009.

[15] G. Brasse, C. Restoin, J. L. Auguste, and J. M. Blondy, "Cascade emissions of an erbium-ytterbium doped silica-zirconia nanostructured optical fiber under supercontinuum irradiation," *Appl. Phys. Lett.*, vol. 94, p. 241903, 2009.

[16] K. Mantey, M. H. Nayfeh, B. Al-Hreish, J. Boparai, A. Kumar, L. D. Stephenson, A. J. Nelson, S. A. Alrokayanm, and K. Abu-Salah, "Silicon nanoparticle-functionalized fiberglass pads for sampling," *J. Appl. Phys.*, vol. 109, p. 064321, 2011.

[17] M. M. Adachi, M. P. Anantram, and K. S. Karim, "Optical properties of crystalline—Amorphous core-shell silicon nanowires," *Nano Lett.*, vol. 10, pp. 4093–4098, 2010.

[18] M. Cazzanelli, D. Navarro-Urrios, F. Riboli, N. Daldosso, L. Pavesi, J. Heitmann, L. X. Yi, R. Scholz, M. Zacharias, and U. Gosele, "Optical gain in monodispersed silicon nanocrystals," *J. Appl. Phys.*, vol. 96, pp. 3164–3171, 2004.

[19] G. P. Kuz'min, M. E. Karasev, E. M. Khokhlov, N. N. Kononov, S. B. Korovin, V. G. Plotnichenko, S. N. Polyakov, V. I. Pustovoy, and O. V. Tikhonevitch, "Nanosize silicon powders: The structure and optical properties," *Laser Phys.*, vol. 10, pp. 939–945, 2000.

[20] P. Roura, J. Farjas, A. Pinyol, and E. Bertran, "The crystallization temperature of silicon nanoparticles," *Nanotechn.*, vol. 18, p. 175705, 2007.

[21] S. G. Dorofeev, A. A. Ischenko, N. N. Kononov, and G. V. Fetisov, "Effect of annealing temperature on the optical properties of nanosilicon from silicon monoxide," *Current Appl. Phys.*, vol. 12, pp. 718–725, 2012.

[22] O. Debieu, "Optical Characterization of Luminescent Silicon Nanocrystals Embedded in Glass Matrices," Ph.D. disserttaion, Friedrich-Schiller Univ., Jena, Germany, 2012.

[23] A. Zwick and R. Carles, "Multiple-order Raman scattering in crystalline and amorphous silicon," *Phys. Rev. B*, vol. 48, pp. 6024–6032, 1993.

[24] X. L. Wu, G. G. Siu, S. Tong, X. N. Liu, F. Yan, S. S. Jiang, X. K. Zhang, and D. Feng, "Raman scattering of alternating nanocrystalline silicon/amorphous silicon multilayers," *Appl. Phys. Lett.*, vol. 69, pp. 523–525, 1996.

[25] P. Melinon, P. Keghelian, B. Prevel, V. Dupuis, A. Perez, B. Champagnon, Y. Guyot, M. Pellarin, J. Lerme, M. Broyer, J. L. Rousset, and P. Delichere, "Structural, vibrational, optical properties of silicon cluster assembled films," *J. Chem. Phys.*, vol. 108, pp. 4607–4613, 1998.

[26] H. Rinnert, M. Vergnat, and A. Burneau, "Evidence of light-emitting amorphous silicon clusters confined in a silicon oxide matrix," *J. Appl. Phys.*, vol. 89, pp. 237–243, 2001.

[27] J. Klangsin, O. Marty, J. Munguia, V. Lysenko, A. Vorobey, M. Pitaval, A. Cereyon, A. Pillonnet, and B. Champagnon, "Structural and luminescent properties of silicon nanoparticles incorporated into zirconia matrix," *Phys. Lett. A*, vol. 372, pp. 1508–1511, 2008.

[28] R. Marczak, J. Judek, A. Kozak, W. Gebicki, C. Jastrzebski, L. Adamowicz, D. Luxembourg, D. Hourlier, and T. Melin, "The individual core/shell silicon nanowire structure probed by Raman spectroscopy," *Phys. Stat. Sol. C*, vol. 6, pp. 2053–2055, 2009.

[29] R. Anthony and U. Kortshagen, "Photoluminescence quantum yields of amorphous and crystalline silicon nanoparticles," *Phys. Rev. B*, vol. 80, p. 115407, 2009.

[30] T. Krishtab, G. G. Gasga, N. Korsunska, M. Baran, S. Kirillova, L. Khomenkova, A. Sachenko, T. Stara, Y. Venger, Y. Emirov, Y. Goldstein, E. Savir, and J. Jedrzejewski, "The peculiarities of $Si/SiO_2$ interafces in the $Si - SiO_2$ systems with Si nanocrystals," *Mater. Sci. Eng. B*, vol. 174, pp. 97–101, 2010.

[31] M. Araya, D. E. Diaz-Droguett, M. Ribeiro, K. F. Albertin, J. Avila, V. M. Fuenzalida, R. Espinoza, and D. Criado, "Photoluminescence in silicon/silicon oxide films produced by the pulsed electron beam ablation technique," *J. Non-Crystal. Solids*, vol. 358, pp. 880–884, 2012.

[32] W. W. Ke, X. Feng, and Y. D. Huang, "Si-nanocrystals with bimodal size distribution in evenly annealed SiO revealed with Raman scattering," *Chin. Phys. Lett.*, vol. 29, p. 016402, 2012.

[33] F. Gourbilleau, C. Ternon, D. Maestre, O. Palais, and C. Dufour, "Silicon-rich $SiO_2/SiO_2$ multilayers: A promising material for the third generation of solar cell," *J. Appl. Phys.*, vol. 106, p. 103501, 2009.

[34] J. Martin, F. Cichos, F. Huisken, and C. von Borczyskowski, "Electron-phonon coupling and localization of excitons in single silicon nanocrystals," *Nano Lett.*, vol. 8, pp. 656–660, 2008.

[35] N. El-Kork, F. Huisken, and C. von Borczyskowski, "Dielectric effects on the optical properties of single silicon nanocrystals," *J. Appl. Phys.*, vol. 110, p. 074312, 2011.

[36] A. M. Chizhik, A. I. Chizhik, R. Gutbrod, A. J. Meixner, T. Schmidt, J. Sommerfeld, and F. Huisken, "Imaging and spectroscopy and electron-phonon coupling in single $SiO_2$ nanoparticles," *Nano Lett.*, vol. 9, pp. 3239–3244, 2009.

[37] X. X. Wang, J. G. Zhang, L. Ding, B. W. Cheng, W. K. Ge, J. Z. Yu, and Q. M. Wang, "Origin and evolution of photoluminescence from Si nanocrystals embedded in a $SiO_2$ matrix," *Phys. Rev. B*, vol. 72, p. 195313, 2005.

[38] R. B. Laughlin and J. D. Joannopoulos, "Phonons in amorphous silica," *Phys. Rev. B*, vol. 16, pp. 2942–2952, 1977.

[39] Y. Kanemitsu, T. Ogawa, K. Shiraishi, and K. Takeda, "Visible photoluminescence from oxidized Si nanometer-sized spheres: Exciton confinement on a spherical shell," *Phys. Rev. B*, vol. 48, pp. 4883–4886, 1993.

[40] T. Shimizu-Iwayama, N. Kurumado, D. E. Hole, and R. D. Townsend, "Optical properties of silicon nanoclusters fabricated by ion implantation," *J. Appl. Phys.*, vol. 83, pp. 6018–6022, 1998.

[41] M. V. Wolkin, J. Jorne, P. M. Fauchet, G. Allan, and C. Delerue, "Electronic states and luminescence in porous silicon qusantum dots: The role of oxygen," *Phys. Rev. Lett.*, vol. 82, pp. 197–200, 1999.
[42] D. S. English, L. E. Pell, Z. Yu, P. F. Barbara, and B. A. Korgel, "Size tunable visible luminescence from individual organic monolayer stabilized silicon nanocrystal quantum dots," *Nano Lett.*, vol. 2, pp. 681–685, 2002.
[43] L. J. Borrero-Gonzalez, L. A. O. Nunes, F. E. G. Guimarae, J. Wojcik, P. Mascher, A. M. Gennaro, M. Tirado, and D. Comedi, "From amorphous to crystalline silicon nanoclusters: Structural effects on exciton properties," *J. Phys.: Condens. Matter*, vol. 23, p. 505302, 2011.
[44] Y. Kanemitsu, N. Simizu, T. Komoda, P. L. F. Hemment, and B. J. Sealy, "Photoluminescent spectrum and dynamics of $Si^{+}$-ion-implanted and thermally annealed $SiO_2$ glasses," *Phys. Rev. B*, vol. 54, pp. 14329–14332, 1996.
[45] E. G. Barbagiovanni, D. J. Lockwood, P. J. Simpson, and L. V. Goncharova, "Quantum confinement in Si and Ge nanostructures," *J. Appl. Phys.*, vol. 111, p. 034307, 2012.
[46] O. A. Shalygina, I. A. Kamenskikh, D. M. Zhigunov, V. Y. Timoshenko, P. K. Kashkarova, M. Zacharias, and M. Fujii, "Optical properties of silicon nanocrystals in silicon dioxide matrix over wide ranges of excitation intensity and energy," *J. Nanoelectron. Optoelectron.*, vol. 4, pp. 147–151, 2009.
[47] B. Averboukh, R. Huber, K. W. Cheah, and Y. R. Shen, "Luminescence studies of a $Si/SiO_2$ superlattice," *J. Appl. Phys.*, vol. 92, pp. 3564–3568, 2002.
[48] E. J. Friebele, G. H. Sigel, Jr., and D. L. Griscom, "Drawing-induced defect centers in a fused silica core fiber," *Appl. Phys. Lett.*, vol. 28, pp. 516–518, 1976.
[49] P. D. Dragic, C. G. Carlson, and A. Croteau, "Characterization of defect luminescence in Yb doped silica fibers: Part I NBOHC," *Opt. Exp.*, vol. 16, pp. 4688–4697, 2008.
[50] A. L. Tomashuk and M. O. Zabezhailov, "Formation mechanisms of precursors of radiation-induced color centers during fabrication of silica optical fiber preform," *J. Appl. Phys.*, vol. 109, p. 083103, 2011.
[51] S. Dhara, C. Y. Lu, K. G. M. Nair, K. H. Chen, C. P. Chen, Y. F. Huang, C. David, L. C. Chen, and B. Raj, "Mechanism of bright red emission in Si nanoclusters," *Nanotechnol.*, vol. 19, pp. 395–401, 2008.
[52] Y. H. Kim, B. H. Lee, Y. Chung, U. C. Paek, and W. T. Han, "Resonant optical nonlinearity measurement of Yb/Al codoped optical fibers by use of a long period fiber grating pair," *Opt. Lett.*, vol. 27, pp. 580–582, 2002.
[53] A. S. Kurkov, Y. E. Sadovnikova, A. V. Marakulin, and E. M. Sholokhov, "All fiber Er-Tm Q-switched laser," *Laser Phys. Lett.*, vol. 7, pp. 795–797, 2010.
[54] I. W. Hsieh, X. Chen, X. Liu, J. I. Dadap, N. C. Panoiu, C. Y. Chou, F. Xia, W. M. Green, Y. A. Vlasov, and R. M. Osgood, Jr., "Supercontinuum generation in silicon photonic wires," *Opt. Exp.*, vol. 23, pp. 15242–15249, 2007.

**Author biographies not included by author request due to space constraints.**